Applied Catalysis B: Environmental 128 (2012) 21–30

Contents lists available at SciVerse ScienceDirect

Applied Catalysis B: Environmental

journal homepage: www.elsevier.com/locate/apcatb

Preferential oxidation of CO (PROX) over CoO_x/CeO_2 in hydrogen-rich streams: Effect of cobalt loading

Preshit Gawade, Burcu Bayram, Anne-Marie C. Alexander, Umit S. Ozkan*

Department of Chemical and Biomolecular Engineering, The Ohio State University 140W. 19th Avenue, Columbus, OH 43210, United States

ARTICLE INFO

Article history:
Received 2 November 2011
Received in revised form 5 June 2012
Accepted 7 June 2012
Available online 8 July 2012

Keywords:
PROX
Cobalt catalyst
Nano ceria
DRIFTS
XANES
XPS

ABSTRACT

PROX reaction over Co catalysts supported on ceria nano-particles was investigated with a special focus on the effect of Co loading. High surface area ceria nano-particles were prepared through a precipitation technique using cerium (III) nitrate hexahydrate and sodium hydroxide. Co incorporation was achieved using a wet impregnation method in aqueous media. Catalysts were characterized using X-ray diffraction, X-ray photoelectron spectroscopy, temperature-programmed reduction, dispersion measurements, and in situ diffuse reflectance Fourier transform infrared spectroscopy and X-ray absorption spectroscopy. Activity and selectivity of CoO_x/CeO_2 catalysts with different Co loadings showed higher Co loadings to favor higher CO oxidation at the expense of oxygen selectivity. Higher activation energies for H_2 oxidation compared to CO oxidation were observed, regardless of the Co loading, implying a higher temperature sensitivity for the H_2 oxidation reaction. The Co phase was identified as Co_3O_4 and was stable in the reducing environments present in PROX reactions.

1. Introduction

Preferential oxidation of CO (PROX) is an important reaction to serve as a connecting link between low-temperature water-gas-shift (LT-WGS) and the proton exchange membrane (PEM) fuel cell. It offers an economical technique for bringing down the carbon monoxide (CO) concentration from 1% to parts per million (ppm) level. PEM fuel cells are popular for their energy efficiency, low operating temperature, compactness and zero-emission. However, the Pt anode used in PEM fuel cells is highly sensitive to CO poisoning and even ppm level of CO can significantly compromise PEM performance. PEM fuel cell is operated around 80 °C [1] whereas, LT-WGS operating range is 200–250 °C [2]. Therefore, 80–200 °C is an ideal temperature window for intermediate PROX step. However, one of the challenges in this temperature range is to selectively oxidize CO with minimal loss of H_2 during side reactions, such as H_2 oxidation and methanation.

Noble metals such as Pt [3–6], Rh/Ru [7], and Ir/Pd [8] are widely studied as PROX catalysts. Pt and Pt-*X* (*X* = Sn, Ce, Co and Ni) supported on various supports, such as Al_2O_3, CeO_2, ZrO_2, CeO_2–ZrO_2, MgO, activated carbon, La_2O_3, SiO_2 and SiO_2–Al_2O_3 [3,6,8–17] are widely investigated for their PROX activity. Pt/CeO_2 is a promising formulation in terms of PROX performance over Pt/Al_2O_3 due to the excellent oxygen storage capacity (OSC) of CeO_2 [3,10], which contributes to better CO oxidation. In addition to these metals, gold is probably as widely studied as Pt-based catalysts for PROX [18–22] due to its higher availability and lower price than Pt [23]. In spite of the promising performance of both Pt- and Au-based catalysts for PROX, inexpensive alternatives are needed.

Copper is the most commonly used non-precious transition metal for PROX catalyst. CuO/CeO_2 and mixed oxides of CuO–CeO_2 are the most widely reported formulations for PROX [24–30]. The synergetic effect between CuO and CeO_2 is known to provide high PROX activity [28,30,31]. Effect of dopant additions has also been investigated for CuO–CeO_2 system [28,32–34].

Cobalt oxide (Co_3O_4) based catalysts are widely studied for CO oxidation in the absence of hydrogen [35–40]. Both, pure Co_3O_4 and Co_3O_4/Al_2O_3 have been reported for high CO oxidation activity in the absence of hydrogen [38,39,41]. When compared with other transition metals, cobalt oxide has better CO oxidation activity as well as selectivity over a wide temperature range in the presence of hydrogen [42]. Several reports in the past [22,43–47] have suggested that cobalt oxide can be a promising candidate for PROX application. It can either provide active sites or can be used as co-dopant in other catalyst formulations. As a co-dopant, it is known to enhance the PROX activity of Au/CeO_2 and Pt/CeO_2. In addition, Omata et al. [48] showed that cobalt supported on alkali earth metal carbonate, such as $Co/SrCO_3$ has excellent PROX activity in the presence of excess hydrogen.

Both, experimental and DFT studies have shown that Co^{3+} is an active site for CO oxidation [39,49,50]. Co^{3+} occupies the octahedral positions in Co_3O_4, which can provide oxygen for CO oxidation

* Corresponding author. Tel.: +1 614 292 6623; fax: +1 614 292 3769.
E-mail address: ozkan.1@osu.edu (U.S. Ozkan).

0926-3373/$ – see front matter © 2012 Elsevier B.V. All rights reserved.
http://dx.doi.org/10.1016/j.apcatb.2012.06.032

resulting in the formation of Co^{2+}. This lower oxidation state cobalt is known to occupy tetrahedral position of Co_3O_4, which may be re-oxidized in the presence of oxygen. However, the deactivation of Co_3O_4 may be observed, if Co^{2+} fails to re-oxidize [39].

Our group [44,45] in the past had studied the various potential supports for Co such as, ZrO_2, CeO_2, Al_2O_3, SiO_2 and TiO_2 for their PROX performance. 10% (wt%) CoO_x catalysts were prepared over commercially available supports using wet-impregnation method. Interestingly, in spite of having extremely low surface area (7 m^2/g) and low Co-dispersion (<0.1%), CoO_x/CeO_2 had shown promising PROX activity. Woods et al. [51] further extended this effort to prepare a high surface are 10% CoO_x/CeO_2 using precipitation and incipient wetness impregnation (IWI) method. The catalyst had high specific surface area (78 m^2/g) and significantly higher Co-dispersion (3.4%) over nano-particles of CeO_2, thereby providing a much improved PROX activity than its previous counterpart.

This work is an extension of our previous studies on PROX catalysis over CoO_x/CeO_2 catalysts. The catalyst preparation method used offers a simpler and cleaner way to prepare high surface area nanoparticles of CoO_x/CeO_2. The effect of Co-loading is examined under hydrogen rich conditions as well as in the presence of CO_2 and water vapor.

2. Experimental

2.1. Catalyst preparation

High surface area ceria nano-particles were prepared through a precipitation technique using cerium (III) nitrate hexahydrate (99.999%, Sigma–Aldrich) and sodium hydroxide. An aqueous solution of cerium nitrate hexahydrate (0.4 M) was mixed with an aqueous solution of sodium hydroxide (2.7 M) at room temperature to form precipitates of $Ce(OH)_2$. The resulting precipitate was aged at room temperature for 24 h followed by washing in de-ionized water until the pH of the filtrate was neutral. The precipitate was, then, dried at 110 °C overnight followed by calcination at 400 °C for 3 h. Cerium oxide support prepared through the precipitation method outlined above yields nano-particles approximately 8 nm in diameter [52].

CoO_x/CeO_2 catalysts with different cobalt loadings were prepared through a wet-impregnation method using aqueous medium. Aqueous solutions of cobalt nitrate hexahydrate of desired concentrations corresponding to 1%, 2% and 10% CoO_x (wt%) loading on the resultant catalysts were prepared at room temperature followed by addition of ceria support into it under constant stirring. The solution was stirred rigorously for 24 h followed by drying at 110 °C. Finally, the catalysts were calcined at 400 °C for 3 h, using a 10 °C/min ramp.

2.2. Catalyst characterization

Micromeritics ASAP 2020 accelerated surface area and porosimetry instrument was used to measure the surface area of support as well as CoO_x/CeO_2 catalysts through N_2 physisorption method at liquid nitrogen temperature (77 K). Before N_2-physisorption, the samples were de-gassed at 130 °C for 12 h at a vacuum better than 3 μm Hg. Brunauer–Emmett–Teller (BET) method was used to determine the specific surface areas of the samples.

The N_2O chemisorption technique outlined earlier in detail [53] was used to obtain the dispersion of cobalt in the CoO_x/CeO_2 catalyst (shown in Table 1). This technique is based on the method developed by Jensen et al. [54] to study the dispersion of Cu over CeO_2. For each run, 100 mg of sample was packed in a fixed bed quartz reactor with a quartz frit bed that is placed inside a fast response furnace (Carbolite, MTF 10/15/130) and pretreated with 5% H_2/He (30 ccm) at 400 °C for 2 h. The reactor was then flushed with He for another 30 min at the same temperature and cooled under helium to 40 °C. Chemisorption of N_2O was carried out by introduction of 4% N_2O/He to the reactor at 40 °C. An on-line mass spectrometer (MKS-Cirrus II) was utilized to monitor the reactor effluents in the m/z = 12 to m/z = 46 range. Prior to the experiment, the mass spectrometer was calibrated for instrumental sensitivity factors and the contribution of the m/z = 28 fragment of N_2O to the m/z = 28 trace. Throughout the experiments, N_2O, N_2 and He were the only species detected in the reactor effluent. The number of moles of N_2 evolved was related to the moles of oxygen consumed and moles of cobalt oxidized by assuming a Co:O stoichiometry of 1:1. As described by Jensen et al. [54], the oxygen uptake is not only due to surface oxidation of Co, but also due to subsurface diffusion. The technique includes a correction for the Fickian diffusion.

Table 1
Specific surface areas and Co dispersions over CoO_x/CeO_2 catalysts.

	Surface area (m^2/g)	Co dispersion (%)	Co surface atoms (μmol/g cat)
CeO_2	123	–	–
1% CoO_x/CeO_2	111	17 ± 2	29
2% CoO_x/CeO_2	106	18 ± 2	62
10% CoO_x/CeO_2	84	21 ± 2	362

Rigaku X-ray diffractometer equipped with Cu Kα radiation source (λ = 1.5418 Å) operated at 40 kV and 25 mA was used to obtain X-ray diffraction patterns of CoO_x/CeO_2 catalysts and CeO_2 support in the range of 20–70°. In situ X-ray diffraction was performed during temperature-programmed reduction of 10% CoO_x/CeO_2 on a Bruker-D8 advanced X-ray diffractometer equipped with an Anton Paar HTK1200 oven using Cu Kα radiation source (λ = 1.5418 Å) operated at 40 kV and 50 mA. The diffraction patterns were collected in the temperature range of 30–700 °C under a flow of 5% H_2/He. International Center for Diffraction Data (ICDD) database was used for the identification of the crystalline phases from the collected diffraction patterns.

Temperature-programmed reduction (TPR) of CoO_x/CeO_2 catalysts, as well as the support, was carried out under a flow of 5% H_2/N_2 (40 ccm). For each run, 100 mg of sample was packed in a quartz reactor with a porous quartz frit. The sample was pretreated in 10% O_2/He (40 ccm) at 400 °C for 1 h, followed by purging with helium at the same temperature for 30 min. The sample was then cooled down to room temperature under the same He flow. Finally, H_2-TPR profile was collected using online mass spectrometer (Cirrus II, MKS Instruments) in 5% H_2/N_2 while increasing the temperature at a rate of 10 °C/min.

Diffuse reflectance infrared Fourier transform spectroscopy (DRIFTS) was performed over CoO_x/CeO_2 samples during PROX. The surface species over CoO_x/CeO_2 as well as the gaseous components were detected using Thermo Nicolet 6700, FT-IR spectrometer equipped with an MCT detector. 28 mg of the sample was loaded to the controlled atmosphere chamber of the DRIFTS instrument for each run. DRIFTS spectra were collected in mid-IR range with resolution of 4 cm^{-1} and averaged over 500 scans. The catalyst was pretreated in 10% O_2/He (40 ccm) for 30 min at 300 °C, followed by cooling of the sample under helium to the desired temperature. Then the background spectrum was collected under helium. Finally, PROX gases (1% CO, 1% O_2, 60% H_2 and helium) were introduced at the same temperature and sample spectra were collected after 10 min under the gas flow.

Kratos AXIS Ultra X-ray photoelectron spectrometer (XPS) equipped with a monochromatic Al Kα radiation source (1486.7 eV) operated at 13 kV and 10 mA was used to study the chemical states of cobalt and/or cerium in the ceria support as well as the

CoO_x/CeO_2 catalysts. A survey scan was collected in the range of 1400–0 eV for every sample at an electron pass energy of 80 eV before sweeping in the Co 2p, Ce 3d and O 1s regions at an electron pass energy of 20 eV. Analysis of the collected X-ray photoelectron spectra was performed using XPS Peak 4.1.

In situ X-ray absorption near edge (XANES) data over 10% CoO_x/CeO_2 was collected at the Co K-edge (7709 eV) at the insertion device beamline (10ID-B) of the Materials Research Collaborative Access Team (MR-CAT) of the Advanced Photon Source, Argonne National Laboratories. The measurements were made in transmission mode and the Si(1 1 1) monochromator was tuned down to eliminate the higher order harmonics in the beam. The catalysts were mixed with SiO_2 at a ratio of 1:2 and finely ground to obtain a homogeneous mixture. A ~30 mg of the mixture was then pelletized in a 6 mm polished steel die and placed inside a 5 cm long quartz tube (6.5 mm ID) and supported with quartz wool plugs. The sample was then centered in an in situ XAFS chamber that was fitted with Kapton® windows and allowed continuous flow of the reactants as well as the isolation of the catalyst sample.

XANES data were collected over the pristine 10% CoO_x/CeO_2 sample in the range of 7500–7750 eV at room temperature. Then the catalyst was pretreated in the presence of 5% O_2/He (20 ccm) at 300 °C for 30 min followed by purging the catalyst with helium at the same temperature for 10 min. The sample was then cooled down to 175 °C under the same He flow. Finally, PROX feed, 0.5% CO, 0.5% O_2, 40% H_2, balance helium (200 ml/min) was introduced at 175 °C for 30 min, followed by in situ XANES data collection at the same temperature. It should be noted that a similar experiment was also attempted over 2% CoO_x/CeO_2 however, lower cobalt concentration coupled with the highly absorbing CeO_2 matrix did not allow collection of XAFS data with sufficient resolution for analysis.

2.3. Catalytic activity testing

Steady-state reactions were performed in a fixed bed reactor flow system using 1/4′ OD stainless steel reactor. For each run, the catalyst was packed inside the reactor using quartz wool and was heated using a homemade, resistively heated furnace. The reaction temperature was measured and controlled by using a K-type thermocouple and an Omega CSC232 PID temperature controller. The reaction feed as well as effluent from the reactor was monitored using on-line micro-GC (Agilent 3000A) equipped with 0.32 mm PLOT mol-sieve and PLOT Q columns with thermal conductivity detectors (TCD) using helium (or argon, when appropriate) as the carrier.

Prior to catalytic activity testing, catalysts were pretreated in situ in 10% O_2/He (30 ccm) at 300 °C for 30 min, followed by cooling to the desired reaction temperature under He flow. Steady-state PROX reaction studies were performed in the temperature range of 100–175 °C at a WHSV (weight hourly space velocity) of 15,000 cm^3 $(g\,cat^{-1})\,h^{-1}$. The feed composition was 1% CO, 1% O_2, 60% H_2 and balance helium.

CO and H_2 oxidation experiments were performed over CoO_x/CeO_2 catalysts using 2% CO (or H_2), 2% O_2 in balance helium (or argon). For these experiments, 50 mg sample was packed inside the reactor and the total flow rate was maintained at 130 ccm to ensure the differential reactor operating conditions. For H_2 oxidation experiments, carrier gas to the micro-GC was replaced with argon to enable detection of hydrogen by the TCD.

The effect of water vapor and CO_2 on the PROX activity of the CoO_x/CeO_2 catalysts was investigated in 125–175 °C ranges at a WHSV of 15,000 cm^3 $(g\,cat^{-1})\,h^{-1}$. The feed composition for these studies was 1% CO, 1% O_2, 60% H_2, 0.5% H_2O (or 0.5% H_2O and 5% CO_2) in balance helium. Water-gas-shift (WGS) and reverse water-gas-shift (RWGS) activity of the CoO_x/CeO_2 formulations were studied in the temperature range of 125–200 °C at a WHSV of 15,000 cm^3 $(g\,cat^{-1})\,h^{-1}$. The feed stream for these studies constituted of 1% CO, 1% H_2O or 5% CO_2, 60% H_2 in helium.

3. Results and discussion

3.1. Surface area and dispersion measurements

Table 1 presents the specific surface area of CoO_x/CeO_2 catalysts with different cobalt loadings. The surface area was found be dependent on the amount of cobalt content and it decreased with increase in cobalt loading. Cobalt dispersion was ~20% regardless of cobalt loadings, suggesting a similar particle size of the Co phase over the support. It should be noted that these dispersion measurements were within ±2% error. Although the particles size seemed to be similar regardless of cobalt loadings, the extent of the support surface populated with these particles or the size of the clusters made of these particles increased with loading.

3.2. Steady state PROX performance of CoO_x/CeO_2

Fig. 1a shows the CO conversion as a function of temperature over CoO_x/CeO_2 catalysts with different cobalt-loadings during preferential oxidation of carbon monoxide. CO conversion was found to increase monotonically with increasing temperature regardless of the cobalt-content. 10% CoO_x/CeO_2 showed slightly better CO oxidation activity than the 2% CoO_x/CeO_2 catalyst especially at temperatures below 150 °C while, the PROX activity of 1% CoO_x/CeO_2 was significantly lower than its counterparts. The difference in the PROX activity diminished at higher temperatures, especially in case of 10% CoO_x/CeO_2 and 2% CoO_x/CeO_2, reaching to approximately 94% of CO conversion at 175 °C over both of these catalysts. In addition, long-term reaction study was performed over 10% CoO_x/CeO_2 for over 40 h at 175 °C as shown in Fig. 1(inset). The data indicated no significant drop in activity or selectivity after the steady state was established in the first 10 h. Co_3O_4 has been considered an excellent candidate for CO oxidation in the presence of hydrogen. However, excess amount of hydrogen under the PROX condition may result in lower oxidation state cobalt phases, including metallic cobalt, which may promote side reactions [42,44,45,48,50,55]. Both these side reactions could result in drop in CO conversion as well as O_2 selectivity to CO_2. However, no such phenomenon was observed during time-on-stream experiment indicating that Co_3O_4 phase was preserved even in the presence of excess hydrogen. This claim was further supported by the X-ray absorption study (Section 3.5.5) where no lower oxidation states of cobalt phases were observed during PROX reaction.

The selectivity of O_2 toward CO_2 is illustrated in Fig. 1b. O_2 selectivity was around 100% in the temperature range of 100–125 °C regardless of cobalt content, indicating negligible hydrogen combustion over these catalysts. However, above 125 °C, O_2 selectivity was observed to decrease for all of the three catalysts, indicating the onset of hydrogen combustion. At 175 °C, O_2 selectivity decreased with increased cobalt loading, indicating that hydrogen combustion was more favored at higher cobalt loadings. For PROX reaction over CoO_x/CeO_2 catalyst, 175 °C was a more relevant reaction temperature as CO conversion reached nearly 100%. Both 10% CoO_x/CeO_2 and 2% CoO_x/CeO_2 showed similar CO conversion at 175 °C, however, O_2 selectivity over 2% CoO_x/CeO_2 was much better (71%) than 10% CoO_x/CeO_2 (58%). Therefore, under the dry PROX conditions, 2% CoO_x/CeO_2 could be a better choice than 10% CoO_x/CeO_2 at 175 °C.

It should be noted that the current CoO_x/CeO_2 catalyst showed superior PROX performance compared to our previously developed [44] cobalt-supported catalysts on various commercial supports such as Al_2O_3, SiO_2, ZrO_2, TiO_2 and CeO_2 (not shown). Furthermore,

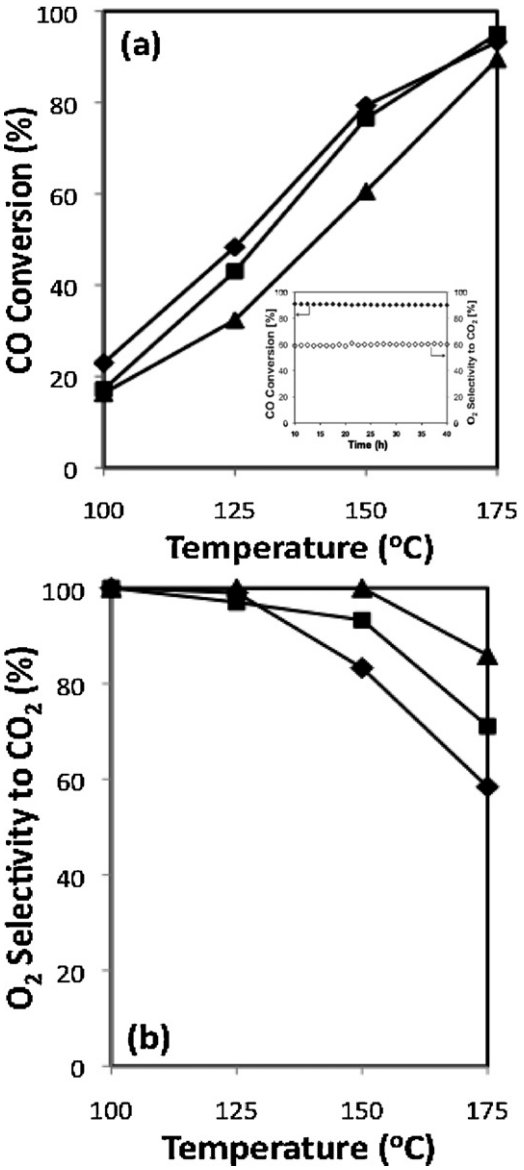

Fig. 1. PROX activity and selectivity of (▲) 1% CoO_x/CeO_2, (■) 2% CoO_x/CeO_2, and (♦) 10% CoO_x/CeO_2. (Reaction conditions: 1% CO, 1% O_2, 60% H_2 in He. WHSV = 15,000 cm^3 $(g\,cat)^{-1}$ h^{-1}.) Inset: Time-on-stream CO conversion and O_2 selectivity to CO_2 over 10% CoO_x/CeO_2 at 175 °C under above mentioned reaction conditions.

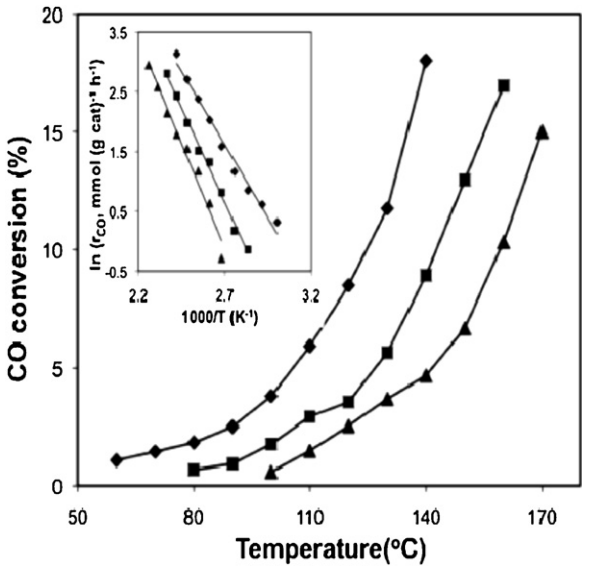

Fig. 2. CO conversion over (▲) 1% CoO_x/CeO_2, (■) 2% CoO_x/CeO_2, and (♦) 10% CoO_x/CeO_2 during CO oxidation. (Reaction conditions: 2% CO and 2% O_2 in helium.) Inset shows Arrhenius plot for determination of the activation energy for CO oxidation.

the PROX performance over the current CoO_x/CeO_2 catalyst was comparable to our previously developed [51] CoO_x/CeO_2 formulation (not shown). However, the current catalyst formulation holds advantages over the previous generation catalysts in terms of ease of synthesis and environmentally benign catalyst preparation.

3.3. Oxidation of CO and H_2 over CoO_x/CeO_2

The kinetics of CO and H_2 oxidation over the CoO_x/CeO_2 catalysts were studied to investigate the intrinsic differences between these catalysts in the presence of excess oxygen. The kinetic data for CO and hydrogen oxidation was collected separately in the presence of 2% CO (or H_2) and 2% O_2. The results obtained during separate CO and H_2 oxidation complement the activity and selectivity data shown in Fig. 1.

Fig. 2 shows the CO conversion over CoO_x/CeO_2 catalysts with different cobalt loadings as a function of temperature during CO oxidation. As expected, CO conversion was found to increase with temperature and cobalt loading. The inset shows the Arrhenius plot for CO oxidation, which was used to obtain activation energies shown in Table 2. The activation energy of CO oxidation was found to increase with decreasing cobalt content. Activation energy numbers indicated that CO oxidation became more difficult in lower cobalt content samples. Therefore, the difference in CO conversion among different CoO_x/CeO_2 catalysts was more prominent at lower temperatures. However, with increase in reaction temperature, sufficient energy appears to have provided in order to overcome the activation energy barrier, consequently difference in activity was diminished at 175 °C.

Fig. 3 shows the H_2 oxidation over CoO_x/CeO_2 catalysts. H_2 oxidation increased with temperature and cobalt content. Arrhenius plot for H_2 oxidation is shown in inset, which was used to obtain activation energies shown in Table 2. The activation energy of H_2 oxidation was found to increase with decreasing cobalt content indicating H_2 oxidation was not favored in samples with low cobalt loading, and hence better O_2 selectivity was achieved over 2% and 1% CoO_x/CeO_2 even at higher reaction temperatures. Furthermore, higher activation energies for H_2 oxidation compared to CO oxidation showed that H_2 oxidation was more temperature sensitive and became more significant at higher PROX temperatures.

3.4. Effect of CO_2 and water vapor over CoO_x/CeO_2

Table 3 compares the CO conversion among CoO_x/CeO_2 catalysts in the presence of water vapor as well as CO_2. The WHSV was maintained at 15,000 cm^3 $(g\,cat^{-1})$ h^{-1} for all the runs. The introduction of 0.5% H_2O in the PROX feed showed the negative effect on CO conversion over CoO_x/CeO_2 catalysts.

Several studies [3,27,46,56] have shown that water vapor can significantly affect the CO conversion due to various reasons, such

Table 2
Activation energies of CO and H_2 oxidation over CoO_x/CeO_2 catalysts.

	CO oxidation (kJ/mol)	H_2 oxidation (kJ/mol)
1% CoO_x/CeO_2	58	93
2% CoO_x/CeO_2	53	80
10% CoO_x/CeO_2	41	65

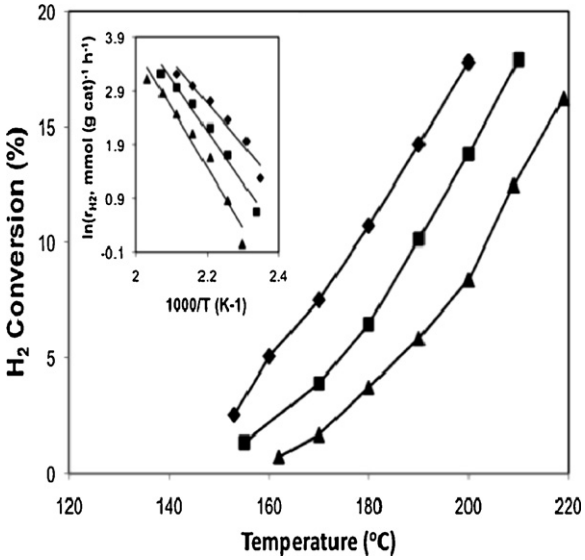

Fig. 3. H_2 conversion over (▲) 1% CoO_x/CeO_2, (■) 2% CoO_x/CeO_2, and (♦) 10% CoO_x/CeO_2 during H_2 oxidation. (Reaction conditions: 2% H_2 and 2% O_2 in argon.) Inset shows Arrhenius plot for determination of the activation energy for H_2 oxidation.

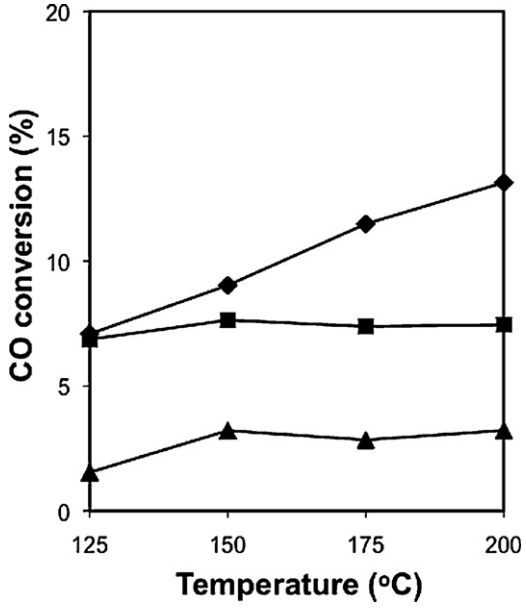

Fig. 4. CO conversion over (▲) 1% CoO_x/CeO_2, (■) 2% CoO_x/CeO_2, and (♦) 10% CoO_x/CeO_2 during water-gas-shift. (Reaction conditions: 1% CO and 1% H_2O in helium.)

as blockage of active site, reverse water-gas-shift (RWGS) and formation of a less active CO–H_2O complex. In our case, this effect was more prominent at lower cobalt content catalysts and low reaction temperatures. 10% CoO_x/CeO_2 was the least affected catalyst in the presence of water vapor at any given temperature between 125 and 175 °C, followed by 2% CoO_x/CeO_2. Performing a water-gas-shift (WGS) reaction over these catalysts in the presence of 1% CO and 1% H_2O supported this observation. As shown in Fig. 4, CO conversion increased with increasing cobalt loading and reaction temperature. 10% CoO_x/CeO_2 had a much better WGS activity compared to other catalysts due to which 95% CO conversion was observed during PROX even in the presence of water.

The combination of 0.5% H_2O and 5% CO_2 in the feed had more significant impact on CO conversion than water alone. Again, 1% CoO_x/CeO_2 was the most affected catalyst followed by 2% CoO_x/CeO_2. CO conversion of 2% CoO_x/CeO_2 dropped to 76% in the presence of CO_2 and H_2O at 175 °C whereas, 10% CoO_x/CeO_2 was still able to achieve around 90% CO conversion. It should be noted that reverse-water-gas-shift (RWGS) was carried out in the presence of 60% H_2 and 5% CO_2 over CoO_x/CeO_2 catalysts (not shown). However, CO_2 conversion was below 3–4% in the temperature range of 100–200 °C indicating that WGS was still a dominant reaction over CoO_x/CeO_2 even in the presence of CO_2, especially over 10% CoO_x/CeO_2.

O_2 selectivites are also presented in Table 3 and were found to decrease in the presence of H_2O and CO_2 at 125 °C indicating that hydrogen oxidation was not as affected as CO oxidation at lower reaction temperatures. However, as the reaction temperature was increased, O_2 selectivites were seen to converge and in the case of 10% CoO_x/CeO_2 and 2% CoO_x/CeO_2 at 175 °C, they showed an increase in the presence of H_2O and CO_2. This observation could be due to increase in CO oxidation and higher WGS reaction rates at higher temperatures, as discussed earlier.

3.5. Catalyst characterization

3.5.1. X-ray diffraction

Fig. 5 shows the X-ray diffraction patterns over CoO_x/CeO_2 catalysts and the bare ceria support collected under ambient conditions. The diffraction lines observed at 2Θ values of 28.44°, 32.96°, 47.56°, 56.2°, 58.6° and 68.9° were assigned to cerianite structure and associated with [1 1 1], [2 0 0], [2 2 0], [3 1 1], [2 2 2] and [4 0 0] planes, respectively. In addition to the cerianite phase, 10% CoO_x/CeO_2 showed distinct diffraction peaks corresponding to cobalt oxide phase (Co_3O_4) located at 2Θ values of 36.7° and 65.15° associated with [3 1 1] and [4 4 0] planes, respectively. Unlike 10% CoO_x/CeO_2, weakly resolved peaks for Co_3O_4 were observed over 2% and 1% CoO_x/CeO_2 along with cerianite phase. This observation along with dispersion measurements indicated that increased in cobalt loading did not change the particle size but the extent of the support surface populated with cobalt particles or the sizes of the clusters made up of these particles. Hence, the surface more populated with Co_3O_4 particles and larger clusters demonstrated diffraction lines with measureable intensities.

Table 3
CO conversion (%) over CoO_x/CeO_2 in the presence of H_2O and CO_2. Values in parentheses show O_2 selectivity to CO_2 (%) over CoO_x/CeO_2 in the presence of H_2O and CO_2.

Temperature		1% CoO_x/CeO_2	2% CoO_x/CeO_2	10% CoO_x/CeO_2
125 °C	No H_2O–CO_2	32 (100)	43 (93)	48 (99)
	0.5% H_2O	19 (82)	31 (91)	34 (93)
	0.5% H_2O–5% CO_2	0 (N/A)	9 (90)	17 (73)
150 °C	No H_2O–CO_2	61 (100)	77 (92)	79 (83)
	0.5% H_2O	50 (94)	70 (92)	78 (83)
	0.5% H_2O–5% CO_2	16 (81)	36 (84)	53 (85)
175 °C	No H_2O–CO_2	89 (86)	95 (70)	93 (58)
	0.5% H_2O	80 (87)	93 (70)	96 (59)
	0.5% H_2O–5% CO_2	53 (86)	77 (83)	88 (65)

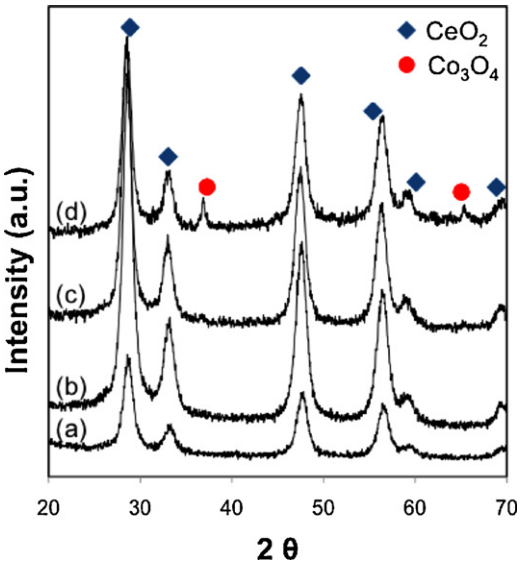

Fig. 5. X-ray diffraction patterns of (a) CeO_2, (b) 1% CoO_x/CeO_2, (c) 2% CoO_x/CeO_2, and (d) 10% CoO_x/CeO_2.

The evolution of the crystal phases under a reducing environment over 10% CoO_x/CeO_2 is shown in Fig. 6. XRD patterns were collected in situ in the presence of 5% H_2/N_2 over calcined 10% CoO_x/CeO_2 in the temperature range of 30–700 °C. The peaks located at 2Θ values of 28.44°, 32.96°, 47.56°, 56.2° and 58.6° are associated with [1 1 1], [2 0 0], [2 2 0], [3 1 1] and [2 2 2], respectively and are characteristic of the cerianite phase. The intensity of cerianite peaks increased with temperature, indicating an increase in average particle size under the reducing environment, especially

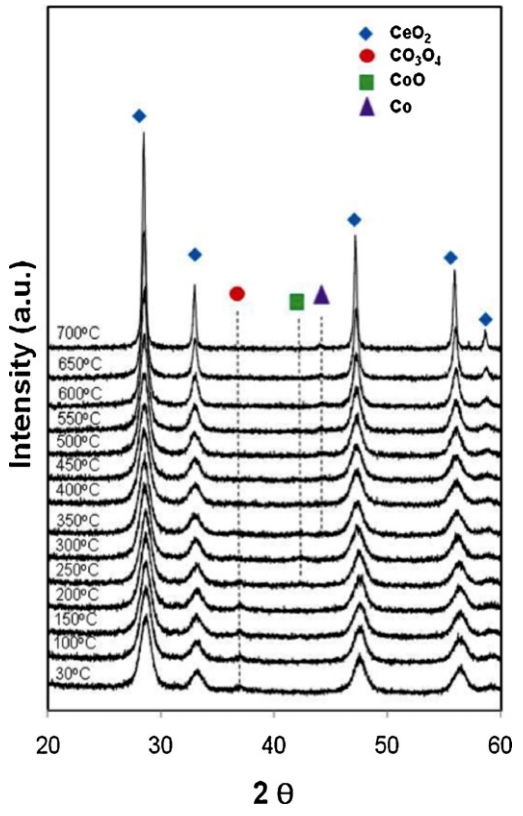

Fig. 6. In situ X-ray diffraction patterns collected during reduction of 10% CoO_x/CeO_2 with 5% H_2/He.

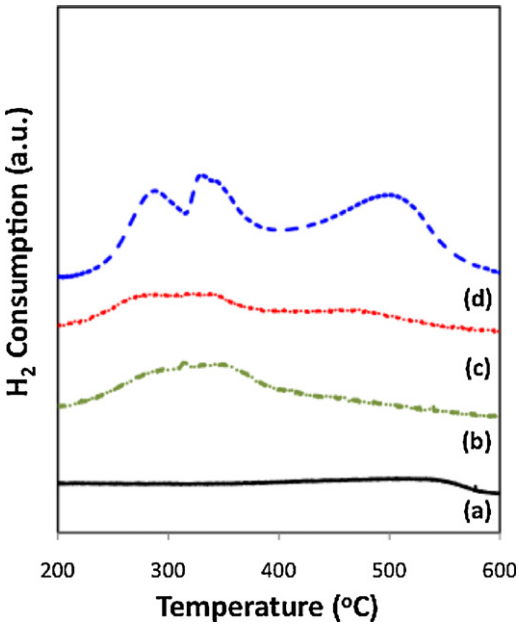

Fig. 7. Temperature-programmed reduction profiles of (a) CeO_2, (b) 1% CoO_x/CeO_2, (c) 2% CoO_x/CeO_2 and (d) 10% CoO_x/CeO_2 in 5% H_2/He.

above 500 °C. The peak at 2Θ value of 36.7° associated with Co_3O_4 [3 1 1] plane started to disappear at 250 °C and a new crystal phase, CoO was observed at 2Θ value of 42.1°. With further temperature increase, CoO started to disappear at 300 °C and metallic cobalt (Co) was observed at 2Θ value of 44.07°.

3.5.2. H_2-TPR

The reduction characteristics of CoO_x/CeO_2 catalysts and CeO_2 support under 5% H_2/He is shown in Fig. 7. A bare CeO_2 support did not exhibit H_2 consumption showing that CeO_2 could not be reduced under the conditions that the TPR was carried out. 10% CoO_x/CeO_2 showed three distinct reduction features at 290 °C, 325 °C and around 500 °C. The reduction peak at 290 °C was assigned to the reduction of Co_3O_4 to CoO whereas the peak at 325 °C was assigned to reduction of CoO to Co [57]. These observations were in good agreement with in situ XRD over 10% CoO_x/CeO_2.

Unlike 10% CoO_x/CeO_2, lower cobalt content catalysts, 2% CoO_x/CeO_2 and 1% CoO_x/CeO_2 showed a broad feature in the temperature of 230–390 °C, which could be correlated to reduction of Co_3O_4 to CoO and CoO to Co. The weakly resolved reduction features observed over these catalysts could be due to low cobalt concentration over CeO_2 support.

The broad peak observed over 10% CoO_x/CeO_2 around 500 °C was assigned to reduction of surface ceria. The transition metals are known to improve the ceria reducibility. In fact, the absence of this reduction feature in 2% CoO_x/CeO_2 and 1% CoO_x/CeO_2 supported the assertion that cobalt was able to improve the reducibility of ceria.

3.5.3. X-ray photoelectron spectroscopy

X-ray photoelectron spectroscopy was used to examine the chemical nature of cerium and cobalt species in CoO_x/CeO_2 catalysts. Fig. 8a–c shows Ce 3d envelope of 1% CoO_x/CeO_2, 2% CoO_x/CeO_2 and 10% CoO_x/CeO_2, respectively. All three spectra showed the contribution from both Ce^{3+} and Ce^{4+}. The peaks labeled as v (884.1 eV), v'' (889.2 eV) and v''' (898 eV) and their corresponding u modes, u (902.7 eV), u'' (907.6 eV) and u'''(916.4 eV) were the characteristic features of Ce^{4+} whereas, v_0 (882 eV), v' (887.2 eV) and their corresponding u modes, u_0 (900.5 eV) and u' (906.6 eV) were the characteristic features of Ce^{3+} species [58–60].

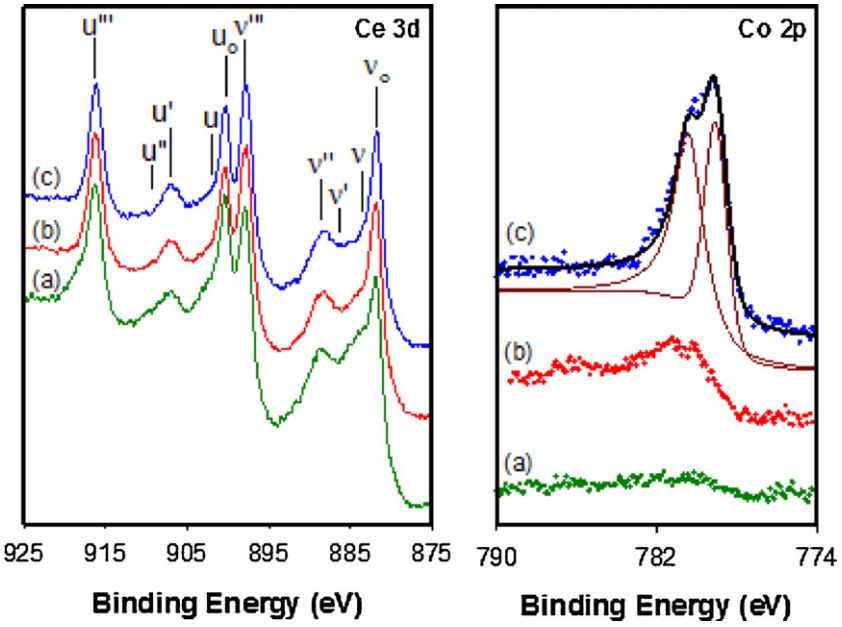

Fig. 8. X-ray photoelectron spectra in the Ce 3d and Co 2p regions of (a) 1% CoO_x/CeO_2, (b) 2% CoO_x/CeO_2 and (c) 10% CoO_x/CeO_2.

Ce 3d envelope showed no significant change upon changing the cobalt loading of the CoO_x/CeO_2 catalysts.

The core-level Co $2p_{3/2}$ spectra of CoO_x/CeO_2 catalysts are shown in Fig. 8. The curve fitting in Co $2p_{3/2}$ region for 10% CoO_x/CeO_2 (Fig. 8c) showed two components located at 779.1 eV and 780.4 eV. The lower binding energy (B.E.) component was assigned to the main photopeak of cobalt oxide (Co_3O_4) whereas, the higher B.E. shoulder at 780.4 eV was associated with Auger LMM transition [61]. For 2% CoO_x/CeO_2 (Fig. 8b), both these peaks were shifted approximately by 1 eV toward higher B.E. values. It is a known fact that binding energy of core-level electrons of Co^{3+} is smaller than that of Co^{2+}. Bonelle et al. [62] explained this phenomenon by postulating that Co^{3+} ions in Co_3O_4 have smaller effective charge than Co^{2+} ions in CoO. Therefore, this final state effect results in a higher binding energy value (usually 0.9 eV apart) of Co^{2+} ions than Co^{3+} ions [63]. In addition, the final state effects in Co 2p region accompany a shift in B.E. of O 1s core-level electrons. The binding energy value of O 1s core electrons in Co_3O_4 is at higher B.E. than CoO [61]. The peak fitting (not shown) in O 1s region for 10% CoO_x/CeO_2 showed the higher B.E. values for O 1s core electron than for 2% CoO_x/CeO_2, supporting this assertion. In addition, the satellite feature was observed at 785.6 eV in 2% CoO_x/CeO_2 along with main photopeak and Auger LMM transition. The presence of the satellite feature in 2% CoO_x/CeO_2 could be due the presence of the paramagnetic Co^{2+} ions [61]. The reduction of cobalt oxide species under X-ray beam in the high-vacuum environment may occur. Therefore it is plausible that some of Co^{3+} ions in Co_3O_4 were reduced to lower oxidation state cobalt oxide. Hence 2% CoO_x/CeO_2 may have some contribution from CoO along with Co_3O_4. In contrast, 10% CoO_x/CeO_2 showed no such evidence of the presence of paramagnetic Co^{2+}, indicating a strong presence of Co^{3+}.

3.5.4. *In situ DRIFTS during PROX over CoO_x/CeO_2 catalysts*

The investigation of surface species formed during PROX over CoO_x/CeO_2 was studied using in situ DRIFTS. Fig. 9a and b shows the in situ DRIFTS spectra collected over 2% CoO_x/CeO_2, at various temperatures, in the presence of 1% CO, 1% O_2, 60% H_2 and helium. The bands associated with gaseous and weakly adsorbed CO were observed at 2152 and 2095 cm^{-1}, respectively, and were seen to decrease with increasing temperature. The doublet of CO_2 at 2358 and 2330 cm^{-1} was found to increase indicating significant CO oxidation at higher PROX temperatures. The strong positive peaks at 1022, 1290 and 1581 cm^{-1} indicate the formation of bidentate carbonate species [64–67] at 30 °C. This observation is consistent with study reported by Luo et al. [64] over Co_3O_4–CeO_2. In their findings, the formation of bidentate carbonates was observed at 1590–1582, 1291–1272 and 1026 cm^{-1} during CO oxidation at room temperature, it was also reported that the intensities of these peaks decreased with increasing temperature. A weak positive feature at 1520 cm^{-1} accompanied by a broad shoulder at 1260–1220 cm^{-1} was also observed at 30 °C, which may be attributed to monodentate carbonate species. Takeguchi et al. [68] also reported monodentate carbonate formation on CeO_2 supports at 1520 and 1270 cm^{-1} after adsorption of both CO and CO_2. Although the presence of monodentate species is to be expected, hydrogen carbonate formation at room temperature cannot be ruled out. Hydrogen carbonate bands have also been reported to occur within the 1270–1220 cm^{-1} region. However these bands are generally accompanied by the additional bands at 1600, 1390–1413 and 1025–1045 cm^{-1} [65,67]. It is possible that these bands are masked due to other carbonates and gas phase species. As the reaction temperature was increased under the PROX feed, the intensities of carbonate bands decreased, possibly due to transformation of carbonate species. The presence of negative bands at 1520, 1220 and 1028 cm^{-1} could suggest that some of the carbonate species were present on the surface when background spectra were collected. The diminished carbonate bands were accompanied by the formation of strong bands at 1463, 1060 and 854 cm^{-1}, which could be assigned to polydentate carbonates. This observation was in agreement with results obtained in a study by Binet et al. [69]. It was reported that adsorption of CO onto ceria at room temperature predominantly results in the formation of bidentate carbonate species, which upon heating convert to polydentate carbonates [69]. In the same study the thermal stability of various carbonate species was discussed and it was found that, the thermal stability increased from bidentate carbonates < monodentate carbonates < polydentate carbonates. Therefore, it is reasonable to believe that bidentate and monodentate carbonates were consumed with an increase in temperature and more stable polydentate species were formed at

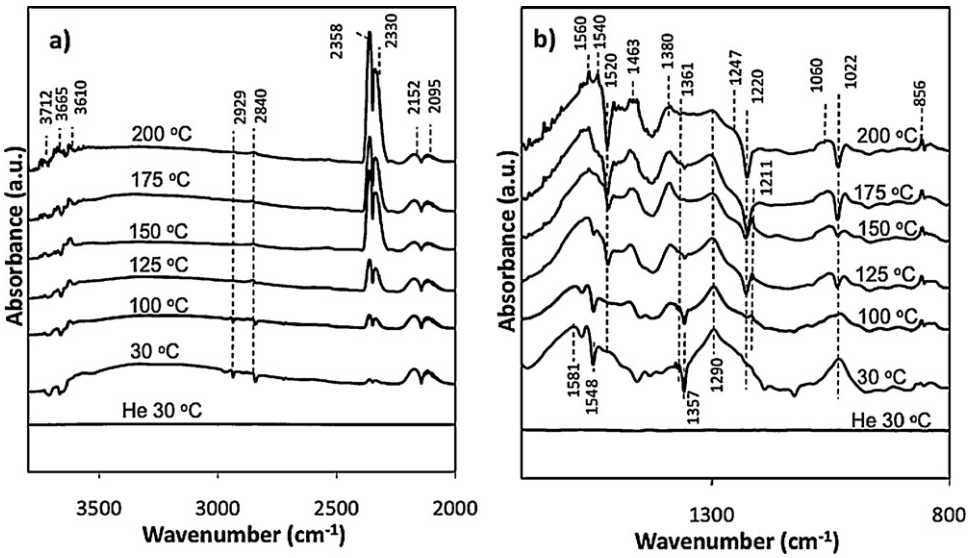

Fig. 9. In situ DRIFT spectra collected during preferential oxidation of CO over 2% CoO_x/CeO_2. (a) High wavenumber region and (b) Low wavenumber region.

higher PROX temperatures. It should be noted that the feature in the range of 1353–1390 cm^{-1} for polydentate carbonate was not observed, most likely due to the presence of a strong broad band at 1380 cm^{-1} which is attributed to the symmetric stretch of CO_2 [65,66]. This was confirmed in a separate experiment (inset in Fig. 10a) where the sample chamber was flushed with He after the catalyst (10% CoO_x/CeO_2) was kept in a PROX reaction medium at 125 °C for 30 min. After the gas phase species were flushed, a sharp band that was observed at 1380 cm^{-1} along with the CO_2 doublet at 2358 and 2330 cm^{-1}diminished with time. Therefore, it is plausible that 1380 cm^{-1} feature was due to symmetric CO_2 stretch. A well-defined positive band at 1211 cm^{-1} was observed at higher temperatures, which could be assigned to the formation of intermediate carbonate species due to adsorption of gas phase CO_2 [64]. The peak at 1403 cm^{-1} usually accompanies this feature, however, the presence of the strong band evidenced at 1380 cm^{-1} due to gaseous CO_2, probably masks this feature. Apart from the carbonates, the formate species were observed with increasing temperature at 2929, 2840, 1560–1540 and 1361 cm^{-1} [45,67,70] which could be due to the interaction OH species at 3712 cm^{-1} (OH-I), 3665 cm^{-1} (OH-II) and 3610 cm^{-1} (OH-III) [67,71] with CO. In addition to the above mentioned formate bands, some negative features were observed at low temperatures around 1548 and 1357 cm^{-1}, which could be assigned to formate species on ceria support [72]. One possibility is that these formate species were present originally on the catalyst when background spectra were collected and were transformed to other species upon introduction of the PROX reaction medium. Nevertheless, there is still some ambiguity in assigning these two negative bands and the possibility of a mathematical artifact due to positive/negative background subtraction cannot be ruled out.

A similar in situ DRIFTS experiment was performed during PROX over 10% CoO_x/CeO_2 as shown in Fig. 10a and b. No significant difference was observed between DRIFT spectra collected over 10% and

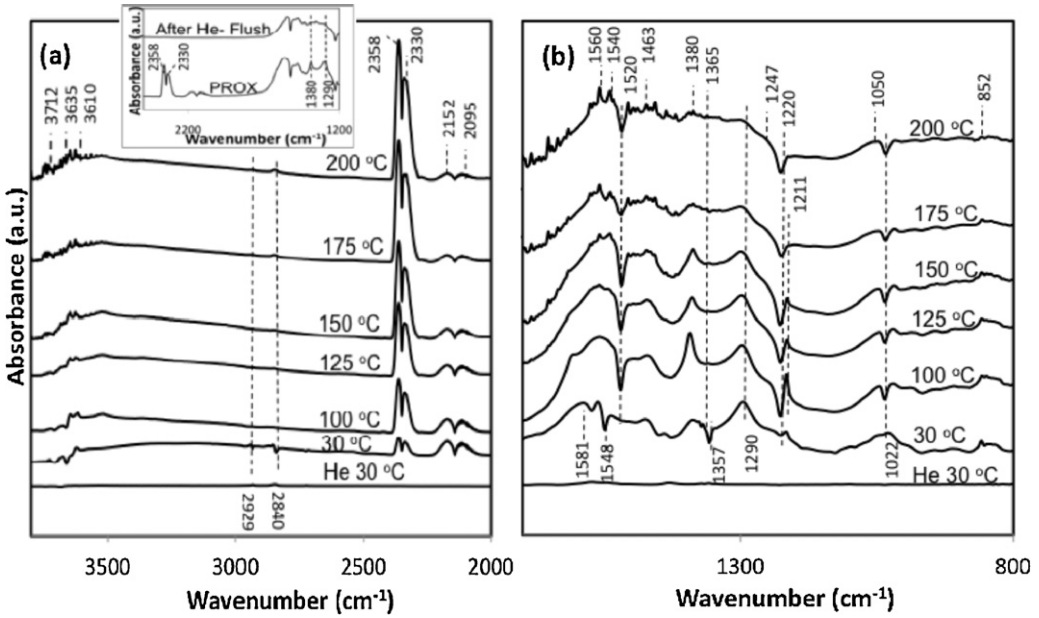

Fig. 10. In situ DRIFT spectra collected during preferential oxidation of CO over 10% CoO_x/CeO_2. (a) High wavenumber region and (b) Low wavenumber region. Inset: spectra taken at 125 °C after the reaction gases are flushed.

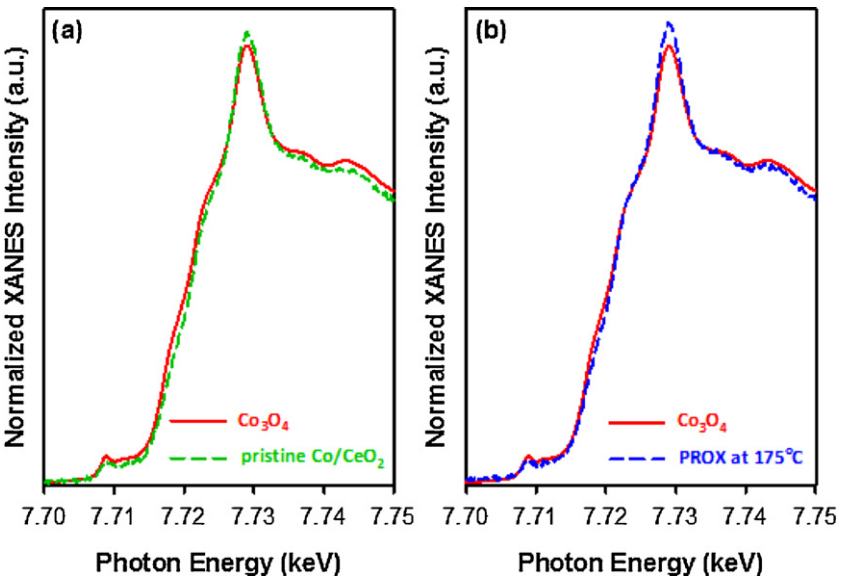

Fig. 11. Normalized Co K-edge XANES spectra of 10% CoO_x/CeO_2. (a) Pristine and (b) In situ under PROX at 175 °C (spectra for Co_3O_4 is included for comparison).

2% CoO_x/CeO_2. However it was noted that the CO_2 doublet occurring at 2356 and 2329 cm^{-1} was more prominent over the 10% CoO_x/CeO_2 sample, suggesting significantly higher CO oxidation. When compared with 2% CoO_x/CeO_2 on common *Y*-axis scale, the intensities of CO_2 doublet were higher in the temperature range of 100–125 °C over 10% CoO_x/CeO_2. However, the difference between CO_2 intensities diminished from 175 °C onwards, in agreement with data presented in Fig. 1. It should be noted that background spectra were collected under helium at each temperature before collecting the sample spectra under PROX feed in order to correct for background CO_2. Therefore, it is reasonable to correlate CO_2 intensities observed during the DRIFTS with CO oxidation activity presented in Fig. 1.

3.5.5. In situ X-ray absorption near edge spectra (XANES)

The transformation of cobalt coordination environment during PROX was monitored using X-ray absorption near edge spectra (XANES). Fig. 11a presents the XANES spectra collected over the pristine 10% CoO_x/CeO_2 in the range of 7500–7750 eV together with Co_3O_4. The XANES spectrum of pristine 10% CoO_x/CeO_2 was well-aligned with Co_3O_4. Fig. 11b presents the XANES spectrum collected during PROX at 175 °C over 10% CoO_x/CeO_2. The XANES spectrum remains similar to that of Co_3O_4 species and reduction of cobalt was not observed.

Several studies in the past have indicated that Co_3O_4 can be an excellent candidate for CO oxidation in the presence of hydrogen. However, the excess hydrogen content during PROX may reduce Co_3O_4 to cobalt oxide phases with lower oxidation states, including metallic cobalt, which may promote the side reactions [42,44,45,48,50,55]. The present study suggests that Co_3O_4 phase remains intact in 10% CoO_x/CeO_2 and no lower valency cobalt was observed during PROX. Having said all this, the possibility of a partial reduction of cobalt species if the catalyst was kept on-line for much longer period or under higher reaction temperatures cannot be ruled out.

4. Conclusions

CoO_x/CeO_2 catalyst was investigated for PROX with a special focus on the effect of cobalt loadings. While higher cobalt loadings favored CO oxidation at low PROX temperatures ($T \leq 150$ °C) under the dry conditions, oxygen selectivity was seen to suffer at higher cobalt loadings. At 175 °C, both 10% CoO_x/CeO_2 and 2% CoO_x/CeO_2 showed nearly 100% CO conversion however, O_2 selectivity over 2% CoO_x/CeO_2 was much better than 10% CoO_x/CeO_2. Furthermore, higher activation energies for H_2 oxidation compared to CO oxidation were observed, regardless of the Co loading, implying a higher temperature sensitivity for the H_2 oxidation reaction. The presence of water and CO_2 in the feed resulted in a drop in PROX performance, possibly due to the inhibition effect over CoO_x/CeO_2 catalyst, regardless of the cobalt loadings. However, higher cobalt loading was seen to demonstrate better water/CO_2 tolerance and assisted water-gas-shift reaction.

The cobalt phase was identified, as Co_3O_4 and was stable in the reducing environments present in PROX reactions. A stable time-on-stream performance over CoO_x/CeO_2 along with catalyst characterization using several analytical techniques indicated no significant contributions from lower valency cobalt species, including metallic cobalt under the reducing environment. The in situ DRIFTS studies conducted on CoO_x/CeO_2 showed that, upon the introduction of PROX reaction gases at room temperature, several species were formed on the catalyst surface such as linearly adsorbed CO, monodentate carbonate and bidentate carbonate species. As the PROX reaction temperature increased, these carbonate species were converted into more stable polydentate carbonates and formate type species. In addition, the intermediate carbonate species were also observed between 100 and 150 °C, probably due to the interaction of adsorbed gas phase CO with the hydroxylated CoO_x/CeO_2 surface.

A tribute to Professor Jean-Marie Herrmann

My co-authors and I feel privileged to be a part of this volume to celebrate Professor Jean-Marie Herrmann's career and his vast contributions to the science of catalysis. His impact on environmental catalysis is well documented through a large volume of publications. But just as important as his scientific achievements, I would say that his true legacy may also lie in all the lives he touched—his students, his colleagues and his friends, that are dispersed all over the world, near and far. When I think of Jean-Marie, what comes to mind is his kindness, his enormous capacity for loving his fellow human beings, his generosity, his loyalty to his friends, his gentle humor, and his incredible knowledge of geography and history of many different civilizations. I will always remember fondly a train

trip we took together from Lyon to Pizza, which made us (me and Christophe Geantet, our other traveling companion) realize that we were traveling with a living encyclopedia and the best teacher in the world.

I feel honored to be able to call Jean-Marie my colleague and my friend. If I have to summarize all his attributes in just a few words, I would say that he is a true scholar and a true gentleman.

Umit S. Ozkan

Acknowledgements

The financial support from Ohio Coal Development Office, the Ohio Department of Development through the Wright Center of Innovation and U.S. Department of Energy through the grant DE-FG36-05GO15033 is gratefully appreciated. Portions of this work were performed at the insertion device beamline (10 ID-B) of the Materials Research Collaborative Access Team (MR-CAT) of the Advanced Photon Source, Argonne National Laboratories. MR-CAT operations are supported by the Department of Energy and the MRCAT member institutions. The use of the Advanced Photon Source at ANL (Argonne National Laboratories) was supported by the U. S. Department of Energy, Office of Science, Office of Basic Energy Sciences, under Contract No. DE-AC02-06CH11357. The authors thank the beamline scientists Tomohiro Shibata and Soma Chattopadhyay for their assistance in collection of the XAFS spectra.

References

[1] M. Krumpelt, T.R. Krause, J.D. Carter, J.P. Kopasz, S. Ahmed, Catalysis Today 77 (2002) 3–16.
[2] J.L. Rangel Costa, G.S. Marchetti, Md.C. Rangel, Catalysis Today 77 (2002) 205–213.
[3] J.L. Ayastuy, A. Gil-Rodríguez, M.P. González-Marcos, M.A. Gutiérrez-Ortiz, International Journal of Hydrogen Energy 31 (2006) 2231–2242.
[4] B. Atalik, D. Uner, Journal of Catalysis 241 (2006) 268–275.
[5] T. Ince, G. Uysal, A.N. Akin, R. Yildirim, Applied Catalysis A: General 292 (2005) 171–176.
[6] E.-Y. Ko, E.D. Park, K.W. Seo, H.C. Lee, D. Lee, S. Kim, Catalysis Letters 110 (2006) 275–279.
[7] S.H. Oh, R.M. Sinkevitch, Journal of Catalysis 142 (1993) 254–262.
[8] F. Mariño, C. Descorme, D. Duprez, Applied Catalysis B: Environmental 54 (2004) 59–66.
[9] H.-S. Roh, H.S. Potdar, K.-W. Jun, S.Y. Han, J.-W. Kim, Catalysis Letters 93 (2004) 203–207.
[10] A. Wootsch, C. Descorme, D. Duprez, Journal of Catalysis 225 (2004) 259–266.
[11] H. Liu, L. Ma, S. Shao, Z. Li, A. Wang, Y. Huang, T. Zhang, Chinese Journal of Catalysis 28 (2007) 1077–1082.
[12] E.-Y. Ko, E.D. Park, K.W. Seo, H.C. Lee, D. Lee, S. Kim, Catalysis Today 116 (2006) 377–383.
[13] G. Uysal, A.N. Akin, Z.I. Onsan, R. Yildirim, Catalysis Letters 108 (2006) 193–196.
[14] C. Pedrero, T. Waku, E. Iglesia, Journal of Catalysis 233 (2005) 242–255.
[15] J. Yan, J. Ma, P. Cao, P. Li, Catalysis Letters 93 (2004) 55–60.
[16] E. Simsek, S. Oezkara, A.E. Aksoylu, Z.I. Onsan, Applied Catalysis A: General 316 (2007) 169–174.
[17] A. Manasilp, E. Gulari, Applied Catalysis B: Environmental 37 (2002) 17–25.
[18] G. Avgouropoulos, M. Manzoli, F. Boccuzzi, T. Tabakova, J. Papavasiliou, T. Ioannides, V. Idakiev, Journal of Catalysis 256 (2008) 237–247.
[19] G. Avgouropoulos, J. Papavasiliou, T. Tabakova, V. Idakiev, T. Ioannides, Chemical Engineering Journal (Amsterdam, Netherlands) 124 (2006) 41–45.
[20] M.M. Schubert, A. Venugopal, M.J. Kahlich, V. Plzak, R.J. Behm, Journal of Catalysis 222 (2004) 32–40.
[21] M.J. Kahlich, H.A. Gasteiger, R.J. Behm, Journal of Catalysis 182 (1999) 430–440.
[22] H. Wang, H. Zhu, Z. Qin, F. Liang, G. Wang, J. Wang, Journal of Catalysis 264 (2009) 154–162.
[23] D. Cameron, R. Holliday, D. Thompson, Journal of Power Sources 118 (2003) 298–303.
[24] J. Papavasiliou, G. Avgouropoulos, T. Ioannides, Applied Catalysis B: Environmental 66 (2006) 168–174.
[25] A. Martínez-Arias, A.B. Hungría, G. Munuera, D. Gamarra, Applied Catalysis B: Environmental 65 (2006) 207–216.
[26] E. Moretti, M. Lenarda, L. Storaro, A. Talon, R. Frattini, S. Polizzi, E. Rodríguez-Castellón, A. Jiménez-López, Applied Catalysis B: Environmental 72 (2007) 149–156.
[27] Y.-Z. Chen, B.-J. Liaw, W.-C. Chang, C.-T. Huang, International Journal of Hydrogen Energy 32 (2007) 4550–4558.
[28] Y.Z. Chen, B.J. Liaw, J.M. Wang, C.T. Huang, International Journal of Hydrogen Energy 33 (2008) 2389–2399.
[29] G. Marban, A.B. Fuertes, Applied Catalysis B: Environmental 57 (2005) 43–53.
[30] P. Ratnasamy, D. Srinivas, C.V.V. Satyanarayana, P. Manikandan, R.S. Senthil Kumaran, M. Sachin, V.N. Shetti, Journal of Catalysis 221 (2004) 455–465.
[31] J.B. Wang, W.H. Shih, T.J. Huang, Applied Catalysis A: General 203 (2000) 191–199.
[32] H. Vidal, J. Kašpar, M. Pijolat, G. Colon, S. Bernal, A. Cordón, V. Perrichon, F. Fally, Applied Catalysis B: Environmental 27 (2000) 49.
[33] Y.Z. Chen, B.J. Liaw, H.C. Chen, International Journal of Hydrogen Energy 31 (2006) 427–435.
[34] Y.Z. Chen, B.J. Liaw, C.W. Huang, Applied catalysis A: General 302 (2006) 168–176.
[35] C.-W. Tang, M.-C. Kuo, C.-J. Lin, C.-B. Wang, S.-H. Chien, Catalysis Today 131 (2008) 520–525.
[36] C.-W. Tang, C.-C. Kuo, M.-C. Kuo, C.-B. Wang, S.-H. Chien, Applied Catalysis A: General 309 (2006) 37–43.
[37] F. Balikci, C. Guldur, Turkish Journal of Chemistry 31 (2007) 465–471.
[38] J. Jansson, Journal of Catalysis 194 (2000) 55–60.
[39] J. Jansson, A.E.C. Palmqvist, E. Fridell, M. Skoglundh, L. Oesterlund, P. Thormaehlen, V. Langer, Journal of Catalysis 211 (2002) 387–397.
[40] J. Jansson, M. Skoglundh, E. Fridell, P. Thormahlen, Topics in Catalysis 16/17 (2001) 385–389.
[41] P. Thormahlen, M. Skoglundh, E. Fridell, B. Andersson, Journal of Catalysis 188 (1999) 300–310.
[42] Y. Teng, H. Sakurai, A. Ueda, T. Kobayashi, International Journal of Hydrogen Energy 24 (1999) 355–358.
[43] C. Kwak, T.-J. Park, D.J. Suh, Applied Catalysis A: General 278 (2005) 181–186.
[44] Z. Zhao, M.M. Yung, U.S. Ozkan, Catalysis Communications 9 (2008) 1465–1471.
[45] M.M. Yung, Z. Zhao, M.P. Woods, U.S. Ozkan, Journal of Molecular Catalysis A: Chemical 279 (2008) 1–9.
[46] Q. Guo, Y. Liu, T. Caputo, L. Lisi, R. Pirone, G. Russo, Reaction Kinetics and Catalysis Letters 92 (2007) 19–25.
[47] L.E. Gómez, I.S. Tiscornia, A.V. Boix, E.E. Miró, Applied Catalysis A: General 401 (2011) 124–133.
[48] K. Omata, Y. Kobayashi, M. Yamada, Catalysis Communications 6 (2005) 563–567.
[49] P. Broqvist, I. Panas, H. Persson, Journal of Catalysis 210 (2002) 198–206.
[50] K. Omata, T. Takada, S. Kasahara, M. Yamada, Applied Catalysis A: General 146 (1996) 255–267.
[51] M.P. Woods, P. Gawade, B. Tan, U.S. Ozkan, Applied Catalysis B: Environmental 97 (2010) 28–35.
[52] P. Gawade, B. Mirkelamoglu, U.S. Ozkan, Journal of Physical Chemistry C 114 (2010) 18173–18181.
[53] H. Song, B. Mirkelamoglu, U.S. Ozkan, Applied Catalysis A: General 382 (2010) 58–64.
[54] J.R. Jensen, T. Johannessen, H. Livbjerg, Applied Catalysis A: General 266 (2004) 117–122.
[55] Z. Zhao, R. Jin, T. Bao, X. Lin, G. Wang, Applied Catalysis B: Environmental 110 (2011) 154–163.
[56] S. Monyanon, S. Pongstabodee, A. Luengnaruemitchai, Journal of the Chinese Institute of Chemical Engineers 38 (2007) 435–441.
[57] H. Song, U. Ozkan, Journal of Molecular Catalysis A: Chemical 318 (2010) 21–29.
[58] M. Romeo, K. Bak, J. El Fallah, F. Le Normand, L. Hillaire, Surface and Interface Analysis 20 (1993) 508–512.
[59] A. Pfau, K.D. Schierbaum, Surface Science 321 (1994) 71–80.
[60] P. Burroughs, A. Hamnett, A.F. Orchard, G. Thornton, Journal of the Chemical Society-Dalton Transactions 1686 (1976) 1686–1698.
[61] J. Haber, L. Ungier, Journal of Electron Spectroscopy and Related Phenomenon 12 (1977) 305–312.
[62] J.P. Bonelle, J. Grimllot, A. D'Huysser, Journal of Electron Spectroscopy and Related Phenomenon 7 (1975) 151.
[63] J.C. Vickerman, I.S. Gilmore, Surface Analysis: The Principle Techniques, 2nd edition, Wiley, 2009.
[64] J.-Y. Luo, M. Meng, X. Li, X.-G. Li, Y.-Q. Zha, T.-D. Hu, Y.-N. Xie, J. Zhang, Journal of Catalysis 254 (2008) 310–324.
[65] M. Daturi, C. Binet, J.C. Lavalley, G. Blanchard, Surface and Interface Analysis 30 (2000) 273–277.
[66] M. Daturi, C. Binet, J.C. Lavalley, A. Galtayries, R. Sporken, Physical Chemistry Chemical Physics 1 (1999) 5717–5724.
[67] O. Pozdnyakova, D. Teschner, A. Wootsch, J. Kroehnert, B. Steinhauer, H. Sauer, L. Toth, F.C. Jentoft, A. Knop-Gericke, Z. Paal, R. Schloegl, Journal of Catalysis 237 (2006) 1–16.
[68] T. Takeguchi, S. Manbe, R. Kikuchi, K. Eguchi, T. Kanazawa, M. Shinichi, W. Ueda, Applied Catalysis A: General 293 (2005) 91–96.
[69] C. Binet, M. Daturi, J.C. Lavalley, Catalysis Today 50 (1999) 207.
[70] H. Kalies, N. Pinto, G.M. Pajonk, D. Bianchi, Applied Catalysis A: General 202 (2000) 197.
[71] A. Badri, C. Binet, J.C. Lavalley, Journal of the Chemical Society-Faraday Transactions 92 (1996) 4669–4673.
[72] E. Finocchio, M. Daturi, C. Binet, J.C. Lavalley, G. Blanchard, Catalysis Today 52 (1999) 53–63.